

# An Accurate Hot Carrier Reliability Monitor for Deep-submicron Shallow S/D Junction Thin Gate Oxide n-MOSFET's

Steve S. Chung, S. J. Chen, C. M. Yih, W. J. Yang, and T. S. Chao\*  
 Department of Electronic Engineering, National Chiao Tung University, Taiwan, R.O.C.  
 \* National Nano Device Lab., Hsinchu, Taiwan, R.O.C.

## ABSTRACT

In this paper, an accurate criterion has been proposed for reliability evaluation of state-of-the-art deep-submicron S/D extension n-MOSFET's. A new monitor for HC reliability evaluation has been developed using total values of  $N_{it}$  in the effective channel length region, instead of commonly used substrate current ( $I_B$ ), impact ionization rate ( $I_D/I_B$ ), or peak/average  $N_{it}$  values. An accurate degradation model has thus been developed based on the  $N_{it}$  distribution and mobility scattering effect. Moreover, this approach has been successfully used to demonstrate the feasibility for gate-engineering studies.

## INTRODUCTION

It has been reported that the drain current degradation of MOSFET is mainly due to the interface state generation [1]. However, there exists an ambiguity that the oxide dependence of this degradation also depends on the device drain structures [2]. For example, the drain current degradation has different gate oxide thickness dependence for conventional and LDD structure MOSFET's. It is known from the measurements that a thinner gate oxide n-channel LDD MOSFET has poorer drain current degradation. It is mainly due to the spacer induced degradation which results from the interface states generated in the spacer region [3]. On contrary to that of LDD MOSFET's, different mechanism exists for conventional single drain MOSFET's. A thinner gate oxide device has better HC reliability for these devices [4]. This smaller degradation is mainly attributed to the smaller mobility reduction due to interface state generation.

On the other hand, the substrate current,  $I_B$  [1], the impact ionization rate,  $I_B/I_D$  [5], and the peak or average value of interface states [6] have been used as a monitor to evaluate HC reliability, which has not been sufficient to accurately correlate  $I_B$  with drain current degradations.

In this paper, we will propose a new and accurate technique to evaluate the hot carrier reliability for the state-of-the-art deep-submicron n-MOSFET's with shallow S/D  $n^+$  extension structure. For these devices, the generated interface states are usually located at the drain extension region inside the gate-drain overlap region. The main degradation mechanism of  $\Delta I_D/I_D$  is mobility degradation in the S/D extension region underneath the gate. An accurate degradation model has thus been developed based on the  $N_{it}$  distribution and mobility scattering effect. Moreover, the same approach has been successfully used to demonstrate the feasibility for gate-engineering studies. The present method is valid for deep-submicron devices with effective channel length down to 0.1 $\mu$ m.

## DEVICE FABRICATION

The devices used in this work were fabricated using 0.25  $\mu$ m CMOS technology (Fig. 1 and Table 1). Two groups of n-MOSFET's were made. Type I has gate oxide thickness of 7nm, 4nm, and 3nm for studying the gate oxide dependence of HC reliability. Type II has 4nm gate oxide thickness and with various pure oxide and  $N_2O$  oxide in combination with RNO spacer. All these n-MOSFET's have shallow S/D  $n^+$  extension. The  $n^+$  S/D extension are formed using implanted Arsenic with dose and energy of  $4.0 \times 10^{14}$   $cm^{-2}$  and 10KeV. Device effective channel lengths are 0.2 $\mu$ m and 0.1 $\mu$ m for types I and II respectively.

Device	Type I			Type II		
	(A)	(B)	(C)	(a)	(b)	(c)
Gate oxide thickness	7nm	4nm	3nm	4nm	4nm	4nm
$L_m(\mu m)/L_{eff}(\mu m)$	0.4/0.2	0.4/0.2	0.4/0.2	0.3/0.1	0.3/0.1	0.3/0.1
Gate oxide material	pure oxide	pure oxide	pure oxide	pure oxide	pure oxide	$N_2O$ oxide
Sidewall spacer material	pure oxide	pure oxide	pure oxide	pure oxide	RNO	RNO

Table 1 Device parameters for test samples used in this study.

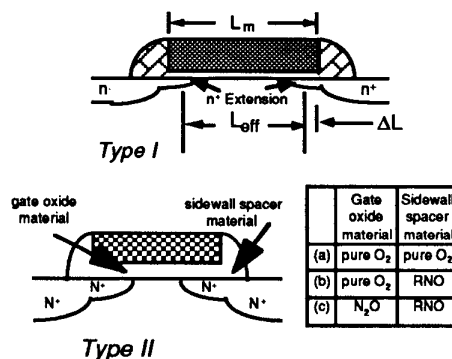


Fig. 1 Two types of MOSFET's used in this study.

## GATE OXIDE THICKNESS DEPENDENCE OF S/D EXTENSION N-MOSFET'S

### Hot Carrier Stress Measurements

For hot carrier stress measurements, maximum substrate current stress conditions,  $I_{B,max}$ , were used. First we measure the substrate currents of three type I devices at  $V_{DS} = 3V$ , as shown in Fig. 2. The impact ionization rates ( $I_B/I_D$ ) are also shown. Then, dc hot carrier stress was performed at  $I_{B,max}$  with  $V_{DS} = 3V$ . This ensures that interface states were generated and no trapped charges were generated [7]. Also, the dominant mechanism of the drain current degradation is interface state. Fig. 3 shows the drain current degradations of these devices with different gate oxide thickness, in which the drain currents were measured at  $V_{GS} - V_T = 1V$  and  $V_{DS} = 0.1V$ . Results show that thinner gate oxide device has smaller drain current degradation. If  $I_B$  is used as a monitor (as in Fig. 2) of HC reliability, we can not identify which oxide thickness device has better reliability since 7nm and 4nm devices have approximately the same peak  $I_B$  values. The device with smaller  $I_B$  will not ensure a smaller  $I_D$  degradation. Therefore, further development of the correlation between drain current degradation, substrate current, and interface states is essential for both drain and gate engineering applications.

### Profiling of Interface States

To solve the aforementioned problems and to find a correct correlation between Fig. 2 and Fig. 3, charge pumping technique [8]

has been employed to calculate the interface state profiles of these devices. Based on a fixed base level charge pumping measurement, the measured CP current is as shown in Fig. 4(a) for fresh and stressed devices, in which  $I_{CP}$  is plotted as  $V_{gh}$  (the applied high level of gate voltage). The difference between 2 curves ( $\Delta I_{CP}$ ) gives the values of  $N_{it}$ . On the other hand, Fig. 4(b) shows the distribution of the local threshold voltage along the channel. Based on the analytical expression (Eq.(5)) of the  $\Delta I_{CP}$  derived in Table 2, we can calculate the spatial distribution of  $N_{it}$ , in which  $dV_{gh}/dx$  can be obtained directly by differentiating  $I_{CP}-V_{gh}$  and  $V_{gh}-x$  can be obtained from simulation. In Table 2,  $f$  is the pulse frequency,  $q$  is electronic charge, and  $W$  is the device channel width. This improved charge pumping method does not need to calculate troublesome depletion width and can characterize the interface states ranged from gate edge to the middle of the channel. Calculated results of the  $N_{it}$  distribution for type I devices are given in Fig.5. Here, the drain junction was determined from simulation. We see that the peak values of  $N_{it}$  distributions are all located inside the drain-gate overlap region and near the drain junction.

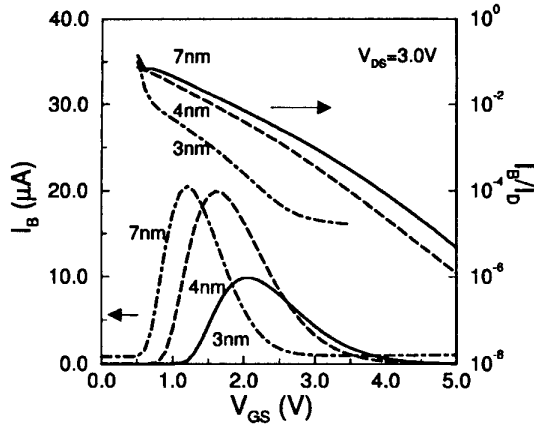


Fig. 2 Measured substrate current  $I_B$  and impact ionization rate ( $= I_B/I_D$ ) for type I devices with different gate oxide thickness. 7nm and 4nm devices have about the same peak values of  $N_{it}$  while 7nm device has larger impact ionization rate.

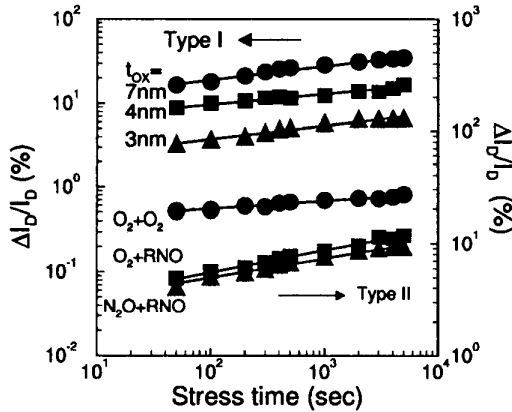


Fig. 3 Measured drain current degradations for type I and type II devices. Both type I and type II were stressed at  $I_{B,max}$  conditions with  $V_{DS}=3V$ .

### Results and Discussion

It is noted that thicker oxide device 7nm shows the largest  $N_{it}$  values which seems to be consistent with the measured drain current degradations in Fig. 2, however, it can not explain the correlation between peak  $N_{it}$  values and  $I_B$  results in Fig. 3 where 7nm has the same value with that of 4nm device. In addition to the interface state

characterization, we use a modified shift and ratio technique [9] to determine the effective channel length of these devices with results given in Fig. 6. Also, the total values of  $N_{it}$  in 7nm device in the effective channel region (Fig. 6) is plotted as a function of the gate voltage drive ( $V_{GS}-V_{TH}-0.5V_{DS}$ ). It is this total  $N_{it,total}$  value (bottom figure of Fig. 6) which causes the largest  $I_D$  degradation.

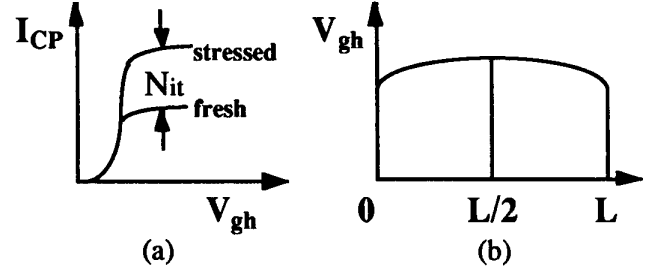


Fig. 4 (a) Schematic diagram showing the measured charge pumping currents for fresh and stressed devices. (b) Schematic diagram of the local threshold voltage distribution along the channel.

$$\Delta I_{CP} = k \int_{V_{gh}}^{V_{gh}} D_{it}(V) dV, \quad k = f \cdot q \cdot W, \quad (1)$$

$$\Delta I_{CP} = k \int_{x_0}^{x_1} D_{it}(V) \frac{dV}{dx} dx, \quad (2)$$

$$\text{let } N_{it}(x) = D_{it}(V) \cdot \frac{dV}{dx}, \quad (3)$$

$$\Delta I_{CP} = k \int_{x_0}^{x_1} N_{it}(x) dx, \quad (4)$$

$$\frac{d\Delta I_{CP}}{dV_{gh}} \frac{dV_{gh}}{dx} = k N_{it}(x), \quad (5)$$

$$\Rightarrow N_{it}(x) = \frac{1}{k} \frac{d\Delta I_{CP}}{dV_{gh}} \frac{dV_{gh}}{dx}. \quad (6)$$

Table 2 Equations used to calculate  $N_{it}$  distributions.

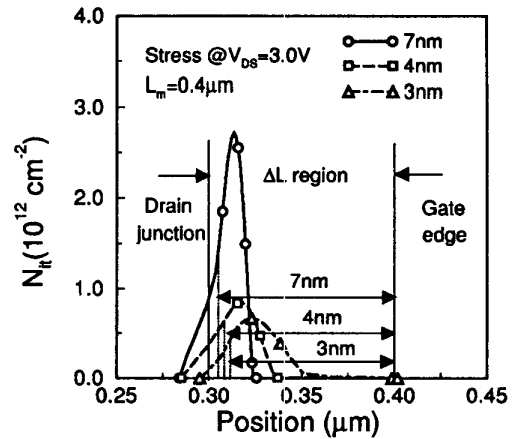


Fig. 5 Extracted  $N_{it}$  distributions for type I device with different gate oxide thickness. 30Å device has smaller number of  $N_{it}$  in the effective channel length region.

The reason for the largest degradation of the 7nm device is explained in Fig. 7, where damaged regions are represented by regions I and II in the channel and spacer regions respectively. The electrical field in a thinner gate oxide device is pushed toward the spacer region and is located inside the gate-drain overlap region. This results in a wider channel length region. Also, much less  $N_{it}$  is covered in the effective channel length region. Thicker oxide device has larger number of  $N_{it}$  covered in region I which yields a larger  $I_D$  degradation. To support this argument, we propose an  $I_D$  degradation model as in Table 3 using a new definition of this  $N_{it}$  effect. Excellent agreement between model and experiment can be achieved as given in Fig. 8. We conclude that thinner gate oxide has smaller  $I_D$  degradation for S/D extension devices based on this total  $N_{it}$  concept. Furthermore, the main degradation of S/D extension device is similar to that of a conventional MOSFET's, in which mobility scattering [6] is the dominant mechanism of drain current degradation. In short, the concept of total  $N_{it}$  values provides a correct monitor for evaluating HC reliability of deep-submicron MOSFET's.

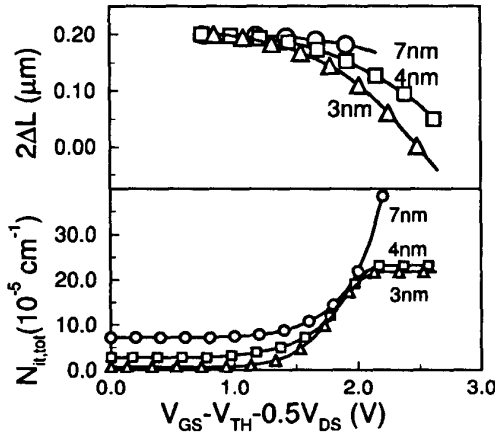


Fig. 6 Effective channel length  $2\Delta L = L_{mask} - L_{eff}$  and total number of interface states  $N_{it}$  inside the effective channel length regions for type I devices with different gate oxide thickness. We see that 70A device has smaller  $L_{eff}$  but the largest total  $N_{it}$  values.

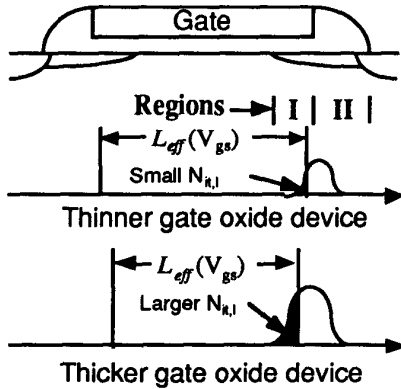


Fig. 7 Illustration of the  $N_{it}$  distributions for devices with thinner and thicker gate oxide thicknesses.

### RELIABILITY FOR GATE-ENGINEERING APPLICATIONS

To improve the reliability of deep-submicron S/D extension devices,  $N_2O$  as the gate oxide and RNO(Reoxidized Nitridation Oxide) as the spacer can achieve this purpose. To show the validity of

the present criterion, reliabilities of type II devices with  $N_2O$  and pure gate oxides were compared. The lower part of Fig. 2 shows the measured  $I_D$  degradation. Fig. 9 shows the measured  $I_B$  and impact ionization rate. Fig. 10 shows the interface state distribution profiles for type II devices. Results show that device (a) has the smallest  $I_B$  but its  $\Delta I_D/I_D$  is the largest. Previous accepted criterion [1] is that device with smaller  $I_B$  should have better reliability, which is in conflict with the results here.

$$\frac{\Delta I_D}{I_D} = \left\{ 1 + \frac{L_{eff}}{\alpha} \left[ \int_0^{L_{eff}} N_{it}(x) dx \right]^{-1} \right\}^{-1} \quad (1)$$

$$\text{where } \mu = \frac{\mu_0}{1 + \alpha N_{it,tot}} \quad (2)$$

$$N_{it,tot} = \int_0^{L_{eff}} N_{it}(x) dx \quad (3)$$

Table 3 A generalized hot carrier model of  $I_D$  degradation for  $n^+$  S/D extension MOSFET's.

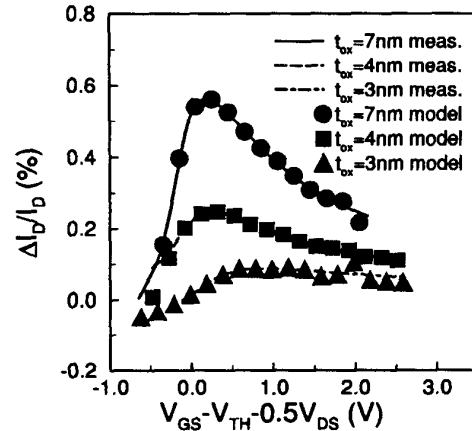


Fig. 8 Measured and modeled drain current degradation for type I (with different gate oxide thickness) devices.

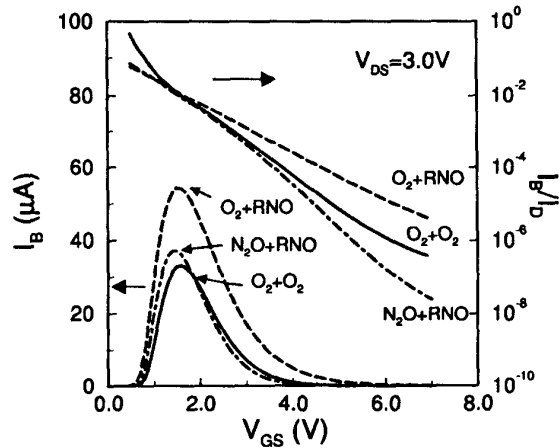


Fig.9 Measured  $I_B$  and impact ionization rate ( $= I_B/I_D$ ) for type II devices with different gate oxide and spacer materials.

By calculating the total values of  $N_{it}$  in the effective channel length region ( $L_{eff} = L_{mask} - \Delta L$ ) (Fig. 11) for three test samples, we found that total values of  $N_{it}$  (bottom figure of Fig. 11) give

(a)>(b)>(c). This means that device (a) has the largest  $N_{it, total}$  values in the effective channel region and hence exhibits poor reliability even though it has smaller  $I_B$ , impact ionization rate, and peak  $N_{it}$  values. In other words, device (a) with pure  $O_2$  gate oxide and  $O_2$  spacer has a wider channel length since its electrical field is pushed toward the gate edge by comparing with those of devices (b) and (c). It has also the largest total values of  $N_{it}$  in Fig. 11 which is consistent with the  $I_D/\Delta I_D$  degradation in Fig. 2. However, it is not consistent with the monitor using  $I_B$  or impact ionization rate in Fig. 9. It further manifests that HC reliability is not appropriate to use  $I_B$  as a monitor since  $N_{it}$  is not proportional to  $I_B$ . The new criterion shown in Fig. 11 or 12 can be used to justify the above reasoning. Again, Fig. 13 shows the comparison of drain current degradation between modeled and measured results for type II devices. Excellent agreement has also been achieved. In short, in terms of the gate-engineering for different gate and spacer oxides, results show that  $N_2O$  as thin gate oxide and RNO as spacer has been proved to be successful for deep-submicron MOSFET's. Furthermore, device with  $O_2$  gate oxide and RNO spacer is most efficient for suppressing the hot carrier effect as revealed in Fig. 10.

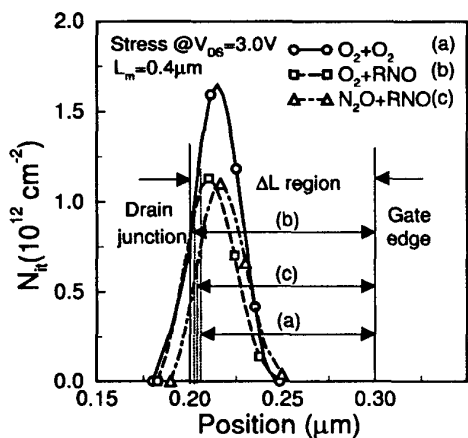


Fig. 10 Extracted  $N_{it}$  distributions for type II devices with different gate oxide materials. Combined  $N_2O$  gate oxide and RNO sidewall spacer has smaller number of  $N_{it}$  in the effective channel length region.

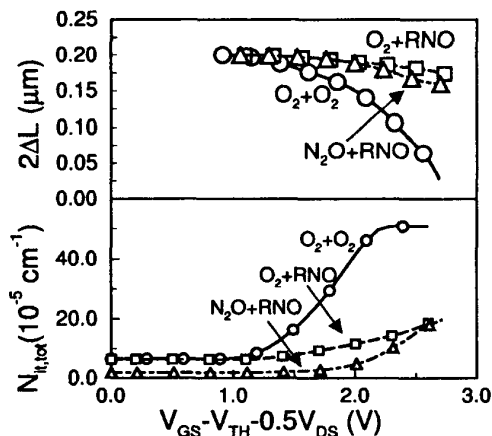


Fig. 11 Effective channel length  $2\Delta L$  and total number of  $N_{it}$  inside the effective channel length regions for different gate oxide and sidewall spacer materials. Note that pure gate oxide and spacer device (a) has the largest number of total  $N_{it}$  in the effective channel due to a wider effective channel length.

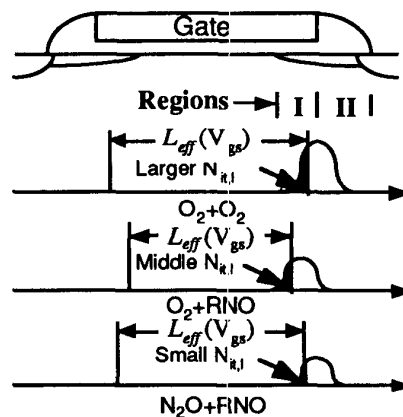


Fig. 12 Schematic diagram to show the comparison of  $N_{it}$  distribution and the effective channel length regions. Device (c) has the smallest number of  $N_{it}$  in the effective channel length region and hence a smallest drain current degradation.

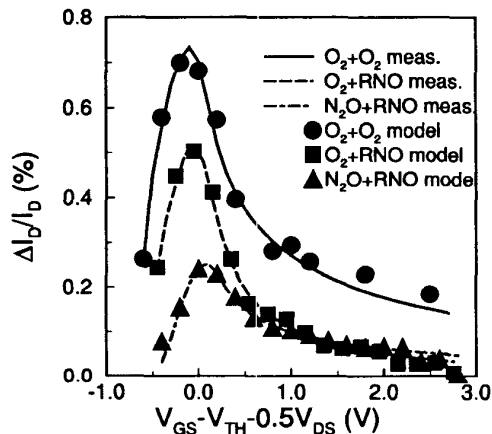


Fig. 13 Comparison of the measured and modeled drain current degradation for type II devices.

In summary, a new and accurate criterion has been proposed for reliability evaluation of deep-submicron n-MOSFET's. Several salient features include: (1) A new monitor for HC reliability evaluation has been proposed using total values of  $N_{it}$  in the effective channel length region, instead of commonly used  $I_B$ ,  $I_B/I_D$ , or peak/average  $N_{it}$  values [1],[5],[6]. (2) The mobility scattering is the dominant factor of  $I_D$  degradation in state-of-the-art S/D extension devices. (3) An analytical  $I_D$  degradation model including the interface state and mobility scattering effect has been developed, and (4) The ambiguity of the HC reliability monitors in thin gate oxide deep-submicron ULSI devices can thus be solved using the present approach.

**Acknowledgments** This work was supported by the National Science Council, Taiwan, under contract NSC86-2215-E009-027.

## REFERENCES

- [1] C. Hu et al., *IEEE T-ED.*, ED-35, p. 375, 1985.
- [2] S. S. Chung et al., *IEEE SISC*, PII.8, Dec. 3-5, 1998.
- [3] F. Hsu, et al., *IEEE EDL.*, EDL-5, p. 71, 1984.
- [4] H. S. Momose et al., in *IEDM Tech. Dig.*, p. 453, 1997.
- [5] T. Hori et al., *IEEE T-ED.*, ED-39, p. 2312, 1992.
- [6] S. Sun et al., *IEEE T-ED.*, ED-27, p. 1497, 1980.
- [7] S. Cheng et al., *IEEE T-ED.*, ED-44, p. 1908, 1997.
- [8] S. Chung et al., *SSDM*, Chiba, Japan, p. 841, 1993.
- [9] S. Biesemans et al., *Symp. VLSI Technology*, p. 166, 1996.